Am J Transl Res 2022;14(4):2212-2230
www.ajtr.org /ISSN:1943-8141/AJTR0134891

Original Article

The Haoqin-Huaban formula alleviates UVB-induced skin damage through HOXA11-AS-mediated stabilization of EZH2

Xuying Xu[1*], Siyi Wang[2*], Dongmei Zhou[2], Jianhua Qu[2], Cang Zhang[2], Yichuan Xu[2], Liyun Sun[2]

Departments of [1]Ulcerative Vascular Surgery, [2]Dermatology, Beijing Hospital of Traditional Chinese Medicine, Capital Medical University, Beijing 100010, China. [*]Equal contributors.

Received May 3, 2021; Accepted December 31, 2021; Epub April 15, 2022; Published April 30, 2022

Abstract: Exposure of skin to ultraviolet B (UVB) irradiation induces oxidative damage, immune suppression, inflammation, and skin cancer. Recently, an increase in the use of traditional Chinese medicine decoction with antioxidant properties has emerged as protection for skin tissues against UVB-induced damage. The aim of this study was to investigate mechanisms of the protective effect of the Haoqin-Huaban formula (HQHB) on UVB-induced skin damage. First, cell survival, apoptosis, and oxidative stress were evaluated upon UVB irradiation in the presence of HQHB using HaCaT cells and mice as model systems. Subsequently, bioinformatic analyses, RNA pulldown assays, RNA immunoprecipitation, luciferase reporter assays, and chromatin immunoprecipitation were conducted to verify the regulation among HQHB, hypoxia-inducible factor 1α (HIF-1α), HOXA11-AS and enhancer of zeste homolog 2 (EZH2) in HaCaT cells. In this study, we found that administration of HQHB inhibited, in a dose-dependent manner, UVB-induced skin damage by eliminating oxidative stress. HQHB was found to upregulate HOXA11-AS expression by activating HIF-1α. Furthermore, HOXA11-AS stabilized the EZH2 protein by inhibiting its ubiquitination and proteasomal degradation. Consequently, rescue assays demonstrated that HOXA11-AS promoted proliferation and inhibited apoptosis in HaCaT cells by reducing oxidative stress. Taken together, our results help to elucidate the function and regulatory mechanism of HQHB in reducing UVB-induced skin damage.

Keywords: Ultraviolet B (UVB) irradiation, Haoqin-Huaban formula (HQHB), HOXA11-AS, enhancer of zeste homolog 2 (EZH2), skin damage

Introduction

Polymorphous light eruption (PLE) is the most common form of photodermatosis, with an incidence as high as 10-20% in the USA and in Western Europe [1]. The principal causative agent of PLE is UVA and/or UVB irradiation [2]. The symptoms of PLE include an intermittent skin reaction, pruritic erythematous papules, vesicles or plaques [3]. The histopathologic features of PLE include a variety of epidermal changes, perivascular lymphocytic infiltrate in the dermis, and subepidermal edema [2]. The etiopathogenesis of PLE remains unclear, but recent studies provide insight into PLE formation, implicating oxidative stress, delayed-type hypersensitivity, and endocrine metabolism [4]. Recent evidence demonstrates that UVB is responsible for oxidative damage as well as DNA single-strand breaks through the generation of malondialdehyde, lipoperoxy radicals, and 4-hydroxy-2-nonenal [5]. Additionally, UVB-induced reactive oxygen species (ROS) interact with multiple cellular targets that regulate several signaling pathways related to cell growth, inflammation, cell survival, and cell differentiation in human keratinocytes [6-8]. Therefore, effective inhibition of oxidative stress will help to alleviate PLE.

Traditional Chinese medicine (TCM) has been a mainstay of the Chinese healthcare system for thousands of years. This accumulated knowledge is the subject of safety and clinical efficacy studies of TCM applied to various diseases [9, 10], and TCM motivates and contributes information to the study of bioactive natural products. Wu et al. [11] reported that Gegen

Qinlian decoction, a prescription of TCM, ameliorates gut toxicity induced by irinotecan chemotherapy in mice by inhibiting oxidative stress and inflammation. The Haoqin-Huaban formula (HQHB) is composed of Herba Artemisiae Annuae, Cornu bubali, Radix rehmanniae, Radix gentianae macrophyllae, Cortex moutan, Radix paeoniae rubra, Radix saposhnikoviae, Radix et Rhizoma Glycyrrhizae. HQHB has been used in clinical treatment of photosensitive skin diseases to good curative effect in China [12]. Previous studies have shown that gallic acid, an active ingredient of *Radix paeoniae rubra*, attenuates LPS-induced oxidative stress and inflammation through the Akt/AMPK/Nrf2 and MAPK/NF-κB pathways [13]. Furthermore, Gou et al. [14] found that total flavonoids from Radix et Rhizoma Glycyrrhizae can reduce hepatic injury and repair liver tissue by improving antioxidant enzyme activity, alleviating inflammation, and reducing oxidative stress. Additionally, an active ingredient of radix rehmanniae, catalpol, was also found to be involved in ameliorating hepatic steatosis and oxidative stress through the p66shc/cytochrome C cascade in LDLr-/- mice [15]. Therefore, we have reason to believe that HQHB can alleviate PLE by ameliorating oxidative stress.

In the present study, the UVB protective effects of HQHB and its mechanism were explored in HaCaT cells and mice to aid in assessing its use in protecting human keratinocytes from UVB-induced oxidative damage. Our results show that HQHB activates HIF-1α and upregulates HOXA11-AS expression, which stabilizes enhancer of zeste homolog 2 (EZH2) protein by inhibiting its ubiquitination and proteasomal degradation. Our findings may lead to novel strategies for protection against light-induced skin damage.

Materials and methods

Animals

Four week old BALB/c mice (50% female and 50% male) were obtained from Tsinghua University (Production License: SCXK (Jing) 2019-0016). Mice were allowed free access to food as well as water and housed in a humidity- and temperature-controlled room (45-55%, 20°C± 2°C). All animal studies adhered to protocols of the Institutional Animal Care facility of Capital Medical University (AEEI-2019-107).

HQHB administration and UVB irradiation

HQHB that met the standards set by the Chinese Pharmacopoeia (2015 Edition) contained Herba Artemisiae Annuae (30 g), Cornu bubali (15 g), Radix rehmanniae (15 g), Radix gentianae macrophyllae (10 g), Cortex moutan (15 g), Radix paeoniae rubra (15 g), Radix saposhnikoviae (6 g), Radix et Rhizoma Glycyrrhizae (6 g). All components were provided by Beijing Shengshilong Pharmaceutical Co., Ltd (Beijing, China). HQHB was dissolved in water to a final volume of 1 L. All the components were extracted by boiling in 400 mL water for 1 h.

We divided 50 mice into 5 groups (10 mice per group). The control groups (ctrl) did not receive treatment. The crude drug (90 g) was diluted 8 fold in drinking water, soaked for 30 min, and decocted for 2 h. The decoction is then filtered and diluted 6 fold in drinking water and further decocted for 1 h. After that, the decoction is concentrated to 80 ml. Before irradiation, mice in the UVB, low, middle and high dose groups were treated orally with sterile saline, 0.5 mL/d, 2 ml/d, or 4 mL/d HFF, respectively, for one week. The dorsal skin of mice in the treatment groups was irradiated after the hair was shaved. Mice were then exposed to UVB (single dose of 80 mJ/cm^2). At a distance of 15 cm, the UV236 irradiation system (Waldmann Medizintechnik, Villingen-Schwenningen, Germany) was used for UVB irradiation with a mean intensity of 2.20 mW/cm^2. The intensity was monitored by a calibrated photometer (Waldmann). Mice were sacrificed and tissue collected 24 h after the final UVB irradiation.

Cell culture and UVB irradiation

HaCaT cells were obtained from the Chinese Academy of Medical Sciences (Beijing, People's Republic of China). HaCaT cells were grown in Dulbecco's Modified Eagle medium (Thermo Fisher Scientific, Inc., Waltham, MA, USA) with 10% (v/v) fetal bovine serum (Thermo Fisher Scientific) in a humidified incubator at 37°C with CO_2 (5% v/v). HaCaT cells were treated with HQHB (10 μL) for 24 h [16]. Subsequently, HaCaT cells were irradiated by UVB (300 mJ/cm^2) for 15 min using the UV236 irradiation system (irradiation intensity: 0.75 mW/cm^2; wavelength: peak =312 nm, range =290-320 nm; distance from source: 15 cm).

Pathologic examination

Hematoxylin-eosin (H&E) staining was conducted using a Hematoxylin and Eosin Staining Kit (Beyotime). Skin tissues were fixed in 10% formaldehyde for one day. Subsequently, dehydration, permeabilization, wax dipping, and paraffin embedding were performed. Then tissues were cut into 3 μm sections. After dehydrating, sections were mounted using neutral gum. Images were obtained by Axio Lab.A1 microscopy (Carl Zeiss AG, Braunschweig, Germany).

For immunohistochemical analyses, skin tissues were fixed using 10% formaldehyde for one day. Subsequently, dehydration, permeabilization, wax dipping, and paraffin embedding were performed. Then the tissues were cut into small pieces, digested with 20 mM proteinase K (5 min), and incubated in methanol (30 min), followed by 3% skim milk. Subsequently, rabbit monoclonal Bcl-2 (1:200; Hangzhou Huabio Biotechnology Co., Ltd, Hangzhou, China) and rabbit monoclonal Bax (1:100; Huabio) antibodies were added. The specimens were than incubated with goat anti-rabbit IgG-HRP (1:200; Huabio). Images were obtained by Axio Lab.A1 microscopy (Carl Zeiss AG). Staining intensity was assessed by three observers as follows: negative (-), weakly positive (+), moderately positive (++), and strongly positive (+++).

TUNEL staining assay

A TUNEL assay for skin tissues was performed using the TUNEL Apoptosis Assay Kit (Beyotime). According to the manufacturer's instructions, skin tissues were cut into 4 μm coronal sections and then into small pieces. Next, tissues were digested with 20 mM proteinase K (5 min). The skin tissues were then incubated with methanol (30 min), followed by 3% skim milk. Subsequently, 50 μL biotin labeling solution was added and incubated for 1 h (37°C), followed by reaction termination solution (0.2 mL) for 10 min (37°C). Then 50 μL streptavidin HRP working solution was added and the specimen incubated for 30 min (37°C), followed by DAB chromogenic solution (0.3 mL) for 10 min (37°C). Next, images were obtained by Axio Lab.A1 microscopy (Carl Zeiss AG). For quantification of TUNEL positive cells, 3 sections were selected from each sample and 5 fields from each section were examined.

Detection of oxidative stress

Total ROS levels in HaCaT cells were detected using the Reactive Oxygen Species Assay Kit (Beyotime). HaCaT cells were suspended in DCFH-DA solution (1.5×10^7 cells/mL) for 20 min. After washing with serum-free medium, fluorescence intensity was measured (emission: 525 nm; excitation: 490 nm). Malondialdehyde (MDA) levels were determined by the Lipid Peroxidation MDA Assay Kit (Beyotime) and following the manufacturer's instructions. Superoxide dismutase (SOD) activity in HaCaT cell lysates was determined using the Total Superoxide Dismutase Assay Kit (Beyotime) and following the manufacturer's instructions. Glutathione peroxidase (GSH-Px) levels in HaCaT cell lysates were detected using the Total Glutathione Peroxidase Assay Kit (Beyotime) and following the manufacturer's instructions.

Plasmid construction

After PCR amplification, cDNA encoding HOXA11-AS was subcloned into the pMSCV-Puro vector (Shanghai Hanbio Biotechnology Co., Ltd, Shanghai, China), which was named HOXA11-AS. The shRNA sequence, specifically targeted to HIF-1α mRNA, was obtained from Hanbio Biotechnology. HaCaT cells (1×10^5 cells) were grown in 3.5-mm dishes. The pMSCV-Puro vector was stably transfected into HaCaT cells and selected with puromycin (1 μg/mL) for 3 days. At 48 h post-transfection, cells were harvested for qRT-PCR or western blot analyses.

RNA extraction and qRT-PCR

Total RNA was extracted from HaCaT cells and skin lesion tissues using the Total RNA Extraction Kit (Beijing Solarbio Science & Technology Co., Ltd, Beijing, China) according to the user guide. In addition, the Cytoplasmic & Nuclear RNA Purification Kit (Shanghai biopike Biotechnology Co., Ltd, Shanghai, China) was utilized to extract cytoplasmic and nuclear RNA from HaCaT cells. Next, the One-Step qRT-PCR Kit (Beyotime) was performed to measure RNA expression according to the manufacturer's instructions. The RNA levels were calculated with the $2^{-\Delta\Delta Ct}$ method and normalized to that of GAPDH. The primers were as follows: HOXA11-AS, F: 5'-CGGCTAACAAGGAGATTTGG-3', R: 5'-AGGCTCAGGGATGGTAGTCC-3'.

GAPDH, F: 5'-ACACCCACTCCTCCACCTTT-3', R: 5'-TTACTCCTTGGAGGCCATGT-3'.

Cell viability analysis

Cell viability of HaCaT cells was measured by the Cell Counting Kit-8 (CCK-8, Beyotime). Briefly, HaCaT cells (2×10^3 cells/well) were seeded into 96-well plates. After treatment for 24 h, fresh medium (90 μL) and CCK-8 reagent (10 μL) were added into each well after decanting the old medium. Then the cells were cultured for 90 min at 37°C. The optical density was measured using a microplate reader (Thermo Fisher Scientific) at a wavelength of 450 nm.

5-Ethynyl-20-deoxyuridine (EdU) incorporation assays were performed using the EdU Cell Proliferation Kit with Alexa Fluor 488 (Beyotime) according to the manufacturer's protocol. HaCaT cells (1×10^6 cells/well) were seeded in 6-well plates after transfection and/or HQHB treatment. Then the same volume of EdU solution was added and incubated for 2 h (37°C). After treatment with 4% paraformaldehyde (15 mins), HaCaT cells were incubated with 0.3% TritonX-100 (15 mins) and click-reactive solution (30 mins). Next, nuclei were counterstained with Hoechst 33342. The percentage of EdU-positive/Hoechst-positive cells was calculated using a FACScan instrument (Becton Dickinson, Mountain View, CA).

For cell apoptosis using the Annexin V-FITC Apoptosis Detection Kit (Beyotime), HaCaT cells were harvested after transfection and/or HQHB treatment. After washing with phosphate-buffered saline (PBS), annexin V-FITC binding solution (195 μL) and annexin V-FITC solution (5 μL) were added, followed by PI (10 μL). After incubation for 20 min at 25°C in the dark, cell apoptosis was detected using a FACScan instrument.

The pharmacological network construction and analysis

The components with oral bioavailability (OB ≥ 30%) and drug-likeness (DL ≥ 0.1) as well as potential targets of Herba Artemisiae Annuae, Cornu bubali, Radix rehmanniae, Radix gentianae macrophyllae, Cortex moutan, Radix paeoniae rubra, Radix saposhnikoviae, Radix et Rhizoma Glycyrrhizae were identified by TCMSP (https://tcmsp-e.com/). Subsequently, using key words including UVB-induced skin damage, actinic prurigo, photosensitivity disorders and sunburn, disease related genes were identified by the Genecards Database (https://www.genecards.org/) and CTD Database (http://ctdbase.org/). The common targets were visualized by Venny 2.1 (https://bioinfogp.cnb.csic.es/tools/venny/index.html). The composition-target network was analyzed through 3.8.2 Cytoscape software (Bethesda, MD, USA) to establish the 'component-target-pathway' network. Nodes in the network represented components of HQHB, common targets, and biological pathways. Using STRING database (https://www.string-db.org/), protein interactions with a confidence score >0.9 were selected in designed setting after eliminating duplicates. Resultant data were obtained from STRING database and introduced into Cytoscape software to establish protein-protein interaction network. Betweenness, bloseness, degree, eigenvector, LAC and network, which indicate the core targets, were analyzed using plug-in components CytoNCA.

Western blotting

HaCaT cells and skin tissues were lysed by cell lysis buffer (Beyotime) supplemented with phosphatase and protease inhibitors (Selleck). In addition, the Nuclear and Cytoplasmic Protein Extraction Kit (Beyotime) was utilized to extract cytoplasmic and nuclear elements from HaCaT cells. After quantification by the Enhanced BCA Protein Assay Kit (Beyotime), cell lysates were separated by SDS-PAGE (10%) and blotted onto PVDF membranes. After soaking in 5% nonfat milk for 60 min, the membranes were incubated with primary antibodies specific to HIF-1α (1:500, Hangzhou Huabio Biotechnology Co., Ltd), EZH2 (1:500, Huabio), Nrf2 (1:1000, Huabio), Lamin B (1:1000, Huabio) and GAPDH (1:5000, Huabio). Horseradish peroxidase-conjugated goat anti-rabbit IgG (1:5000, Huabio) was added. Lamin B and GAPDH were used as an internal reference. The results were measured following treatment with a chemiluminescent HRP substrate (Merck Millipore, Hong Kong, China) and analyzed using the ImageJ 7.0 software (National Institutes of Health, Bethesda, MD, USA).

Dual-luciferase reporter assay

HOXA11-AS mRNA promoter sequences and mutant promoter sequences of chr7:27185454-27185465 were subcloned into the luciferase reporter gene vectors pGL3 plasmids (Wuhan GeneCreate Bioengineering Co., Ltd, Wuhan, China). An empty pcDNA3.1 vector was used as a control. pcDNA3.1 plasmid and shRNA were cotransfected into HEK-293T cells using Lipofectamine 2000 (Thermo Fisher Scientific) in 24-well plates. After 32 hours, the ratio between firefly and Renilla luciferase activity (Fluc/Rluc) was measured.

Chromatin immunoprecipitation (ChIP) assays

The interaction between HIF-1α and HOXA11-AS1 promoter was verified by the Plus Enzymatic Chromatin IP Kit (Cell Signaling Technology, Inc., USA). Chromatin was crosslinked with formaldehyde (1%), followed by sonication to generate DNA fragments (200- to 500-bp). Then appropriate antibodies were utilized to immunoprecipitate the protein-DNA complex. The protein-DNA complexes were reversed by NaCl (5 M). DNA was extracted by phenol/chloroform, followed by precipitation with ethanol and glycogen. Subsequently, purified DNA was measured using qRT-PCR.

RNA pull-down assay

RNA pull-down assays were performed by the Pierce Magnetic RNA-protein pull-down kit (Thermo Fisher Scientific) according to the manufacturer's instructions. Subsequently, 50 μM biotinylated HOXA11-AS or anti-sense were transfected into HaCaT cells by Lipofectamine 2000. After 24 h, HaCaT cells (1×10^6 cells) were lysed, followed by sonication and centrifugation. Next, HaCaT cells were incubated with streptavidin-coated magnetic beads (Thermo Fisher Scientific) at 4°C for 60 min. Proteins bound to HOXA11-AS1 were measured using western blotting.

RNA immunoprecipitation (RIP) assay

The interaction between EZH2 and HOXA11-AS1 was verified by the RNA Immunoprecipitation Kit (Guangzhou Geneseed Biotechnology Co., Ltd, Guangzhou, China). In brief, HaCaT cells (1×10^6 cells) were lysed, followed by incubation with RIP buffer supplemented with magnetic beads conjugated to antibodies against EZH2 (Huabio) or anti-rabbit IgG (Huabio). HOXA11-AS1 levels were detected using qRT-PCR. Total RNA was used as a control.

Statistical analysis

All data were obtained from three independent experiments. Data are expressed as mean ± standard deviation. Statistical analysis was carried out using SPSS 20.0 software (SPSS Inc., Chicago, IL, USA). Student's t test was used to analyze the difference between two groups. One-way ANOVA followed by Tukey's test was used to analyze the difference among multiple groups. $P<0.05$ was recognized as statistically significant.

Results

Haoqin-Huaban granules alleviate UVB-induced skin damage

We first investigated the protective effects of HQHB on UVB-induced skin damage in Balb/c mice. UVB irradiation (80 mJ/cm^2 for 24 h) caused edema, redness, and general disruption of skin integrity. In mice treated with the HQHB, however, UVB irradiation resulted in little skin redness, edema, change in thickness or other structural disruption (**Figure 1A**). The thickness of the epidermis in mice irradiated by UVB was 64.07±7.38 μm, which was significantly greater than in control mice (30.75±4.37 μm). Fourteen days after HQHB administration, the thickness of the epidermis exhibited a dose-dependent decrease to 51.07±4.74 μm (0.5 ml/d), 43.64±3.45 μm (2 ml/d) and 37.07±2.32 μm (4 ml/d). All thicknesses were significantly lower than in mice following UVB irradiation alone ($P<0.01$, **Figure 1B**). The above observations of changes in epidermal thickness and skin integrity were confirmed by H&E staining (**Figure 1C**). Cell apoptosis *in vivo* at 24 h after UVB irradiation is shown in **Figure 1D**, **1E**. Many apoptotic cells with dark brown and TUNEL-positive nuclei were observed in the UVB group. However, HQHB administration effectively reduced the number of apoptotic cells in a dose-dependent manner. Levels of apoptosis-related proteins in each group of mice are shown in **Figure 1F**, **1G**. As shown by immunohistochemical analysis, UVB irradiation significantly increased the expression of Bax and decreased that of Bcl-2. However, HQHB

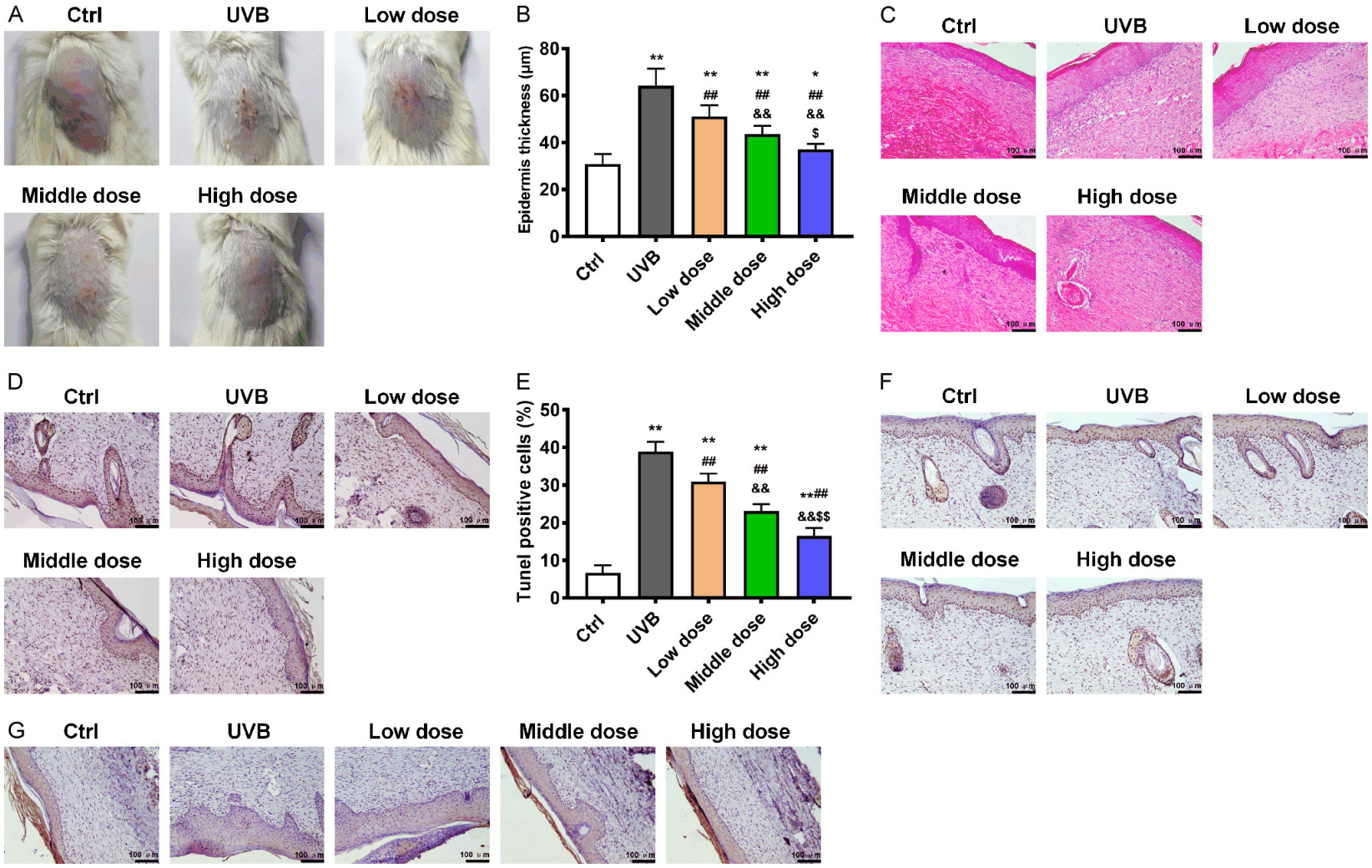

Figure 1. HQHB reverses UVB-induced skin damage. A. Macroscopic changes in mouse skin. B. Epidermal thickness was measured with a digimatic caliper. *P<0.05, **P<0.01 vs Ctrl; $^{\#}$P<0.05, $^{\#\#}$P<0.01 vs UVB; $^{\&}$P<0.05, $^{\&\&}$P<0.01 vs Low dose; $^{\$}$P<0.05, $^{\$\$}$P<0.01 vs Middle dose. C. H&E-stained sections showing epidermal tissues after different treatments. Scale bars, 100 μm. D and E. Representative TUNEL-stained sections showing epidermal tissues after different treatments. Scale bars, 100 μm. *P<0.05, **P<0.01 vs Ctrl; $^{\#}$P<0.05, $^{\#\#}$P<0.01 vs UVB; $^{\&}$P<0.05, $^{\&\&}$P<0.01 vs Low dose; $^{\$}$P<0.05, $^{\$\$}$P<0.01 vs Middle dose. F. Bax expression in sections of epidermal tissues after different treatments was determined by immunohistochemistry. Scale bars, 100 μm. G. Bcl-2 expression in sections of epidermal tissues after different treatments was determined by immunohistochemistry.

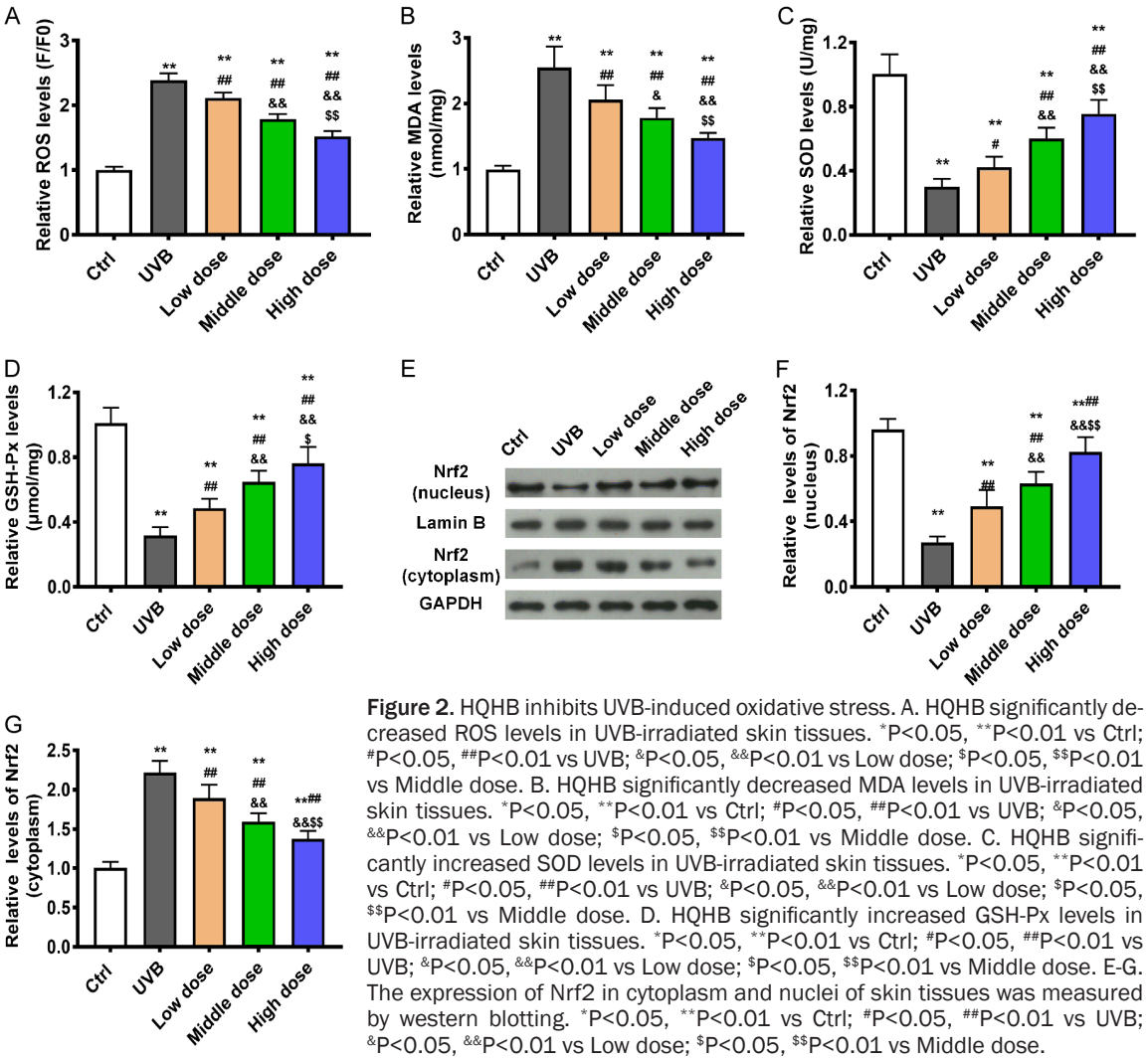

Figure 2. HQHB inhibits UVB-induced oxidative stress. A. HQHB significantly decreased ROS levels in UVB-irradiated skin tissues. *P<0.05, **P<0.01 vs Ctrl; #P<0.05, ##P<0.01 vs UVB; &P<0.05, &&P<0.01 vs Low dose; $P<0.05, $$P<0.01 vs Middle dose. B. HQHB significantly decreased MDA levels in UVB-irradiated skin tissues. *P<0.05, **P<0.01 vs Ctrl; #P<0.05, ##P<0.01 vs UVB; &P<0.05, &&P<0.01 vs Low dose; $P<0.05, $$P<0.01 vs Middle dose. C. HQHB significantly increased SOD levels in UVB-irradiated skin tissues. *P<0.05, **P<0.01 vs Ctrl; #P<0.05, ##P<0.01 vs UVB; &P<0.05, &&P<0.01 vs Low dose; $P<0.05, $$P<0.01 vs Middle dose. D. HQHB significantly increased GSH-Px levels in UVB-irradiated skin tissues. *P<0.05, **P<0.01 vs Ctrl; #P<0.05, ##P<0.01 vs UVB; &P<0.05, &&P<0.01 vs Low dose; $P<0.05, $$P<0.01 vs Middle dose. E-G. The expression of Nrf2 in cytoplasm and nuclei of skin tissues was measured by western blotting. *P<0.05, **P<0.01 vs Ctrl; #P<0.05, ##P<0.01 vs UVB; &P<0.05, &&P<0.01 vs Low dose; $P<0.05, $$P<0.01 vs Middle dose.

administration significantly reversed these effects in a dose-dependent manner.

Haoqin-Huaban granules attenuate oxidative stress

We investigated whether HQHB attenuates oxidative stress in UVB-irradiated mice. The elevated MDA and ROS levels in UVB-irradiated mice was clearly attenuated by HQHB in a dose-dependent manner (P<0.01, **Figure 2A**, **2B**), indicating that HQHB is capable of controlling lipid peroxidation and ROS generation. Furthermore, we investigated the role of HQHB on antioxidant enzymes in UVB-irradiated mice. The activities of SOD and GSH-Px in skin tissues were suppressed in UVB-irradiated mice (P<0.01, **Figure 2C**, **2D**), indicating an impaired antioxidant defense system. One week after HQHB application, the activities of SOD and GSH-Px were partially reversed (P<0.01). The activities of antioxidants in UVB-irradiated mice receiving HQHB significantly increased with increasing HQHB concentration (P<0.01, **Figure 2C**, **2D**), indicating that HQHB has the ability to restore the impaired antioxidant defense system. In addition, we assessed Nrf2 expression following UVB irradiation (80 mJ/cm^2 for 24 h) and observed a marked elevation in the cytoplasm and reduction in the nucleus (**Figure 2E**, **2G**); HQHB treatment reversed these changes. Together, these results indicate that HQHB attenuates UVB-induced skin damage by inhibiting oxidative stress.

HQHB component-target network construction

Next, we investigated the mechanism whereby HQHB affects oxidative stress through the network pharmacology. The components and

potential targets of Herba Artemisiae Annuae, Cornu bubali, Radix rehmanniae, Radix gentianae macrophyllae, Cortex moutan, Radix paeoniae rubra, Radix saposhnikoviae, Radix et Rhizoma Glycyrrhizae, which constitutes HQHB, were identified as shown in Table S1. After screening with OB and DL, a total of 173 components were obtained from the TCMSP. 287 possible targets of these components were also obtained from the TCMSP. Subsequently, a total of 424 genes related with UVB-induced skin damage were obtained from the Genecards Database (458 genes) and CTD Database (15544 genes), shown in **Figure 3A** and Table S2. Furthermore, a total of 92 genes, which were both related to HQHB and UVB-induced skin damage, were identified by Venn diagrams (**Figure 3B** and Table S3). As shown in **Figure 3C**, the compound-target network was structured, which composed of 231 nodes and included 173 bioactive compounds and 92 targets. Subsequently, the proposed inter-protein interactions among the targets associated with disease and HQHB were constructed and shown in **Figure 3D**. After hiding disconnected nodes, there are 172 nodes and 754 edges in the network. Additionally, betweenness, bloseness, degree, eigenvector, LAC and network, which are regarded as crucial nodes and used to assess the essence of the whole network, were identified by the numbers of interactions (28 nodes and 306 edges). As shown in **Figure 3D**, HIF-1α was one of the most important targets in the network.

Haoqin-Huaban granules upregulate HOXA11-AS expression through HIF-1α

Interestingly, HQHB administration significantly increased the levels of phosphorylation of HIF-1α in a dose-dependent manner (P<0.01), but not the levels of HIF-1α itself (**Figure 4A**, **4B**), indicating that the antioxidant effects of HQHB may occur by downstream targets of HIF-1α. Next, from a search of the online bioinformatics website ChIPBase v2.0 (http://rna.sysu.edu.cn/chipbase/index.php), 180 potential long non-coding RNA (lncRNA) sites of HIF-1α binding were found. We were particularly interested in lncRNA HOXA11-AS (**Figure 4C**, **4D**). We examined lncRNA expression levels and found that expression of HOXA11-AS was significantly upregulated in UVB-irradiated mice treated with HQHB compared with mice treated with UVB irradiation alone (P<0.01, **Figure 4E**). Knockdown of HIF-1α led to a significant decrease in HOXA11-AS expression in HaCaT cells (P<0.01, **Figure 4F**, **4G**). To confirm HOXA11-AS was a transcriptional target of HIF-1α, we co-transfected luciferase reporter and shRNA against HIF-1α into HEK-293T cells. The results showed that HIF-1α knockdown significantly reduced luciferase activity of the chr7:2718-5454-27185465 fragment; however, luciferase activity of a reporter containing chr7:271-85754-27185765 was not affected (P<0.01, **Figure 4H**). In addition, the ChIP database indicated that HIF-1α had a strong affinity in its promoter region for HOXA11-AS (**Figure 4I**). These data suggested that HIF-1α upregulated HOXA11-AS expression in HaCaT cells by transcriptionally activating HOXA11-AS.

HOXA11-AS suppressed UVB-induced cell damage

To investigate the effects of HOXA11-AS on UVB-induced cell damage, we stably overexpressed HOXA11-AS in HaCaT cells (**Figure 5A**). CCK8 assays showed that the reduced cell viability of HaCaT cells was significantly attenuated by HOXA11-AS, and was further significantly attenuated by the combination of HOXA11-AS overexpression and HQHB administration (all P<0.01, **Figure 5B**). Similar results were found in EdU incorporation assays (**Figure 5C**, **5D**). Furthermore, we analyzed whether HOXA11-AS can alleviate UVB-induced apoptosis. Flow cytometry showed that HOXA11-AS was capable of ameliorating UVB-induced apoptosis (P<0.01, **Figure 5E**, **5F**) as did TUNEL staining (P<0.01, **Figure 5E**, **5G**). In addition, the decreased apoptosis rate induced by HOXA11-AS was further significantly decrease by the combination of HOXA11-AS overexpression and HQHB administration (P<0.01, **Figure 5E**, **5F**) as did TUNEL staining (P<0.01, **Figure 5E**, **5G**). Interestingly, the elevated ROS and MDA levels in UVB-irradiated cells were significantly attenuated by HOXA11-AS overexpression with/without HQHB administration (P< 0.01, **Figure 6A**, **6B**). Furthermore, we found that the suppression of antioxidant enzymes in HaCaT cells irradiated by UVB was reversed by overexpression of HOXA11-AS with/without HQHB administration (P<0.01, **Figure 6C**, **6D**).

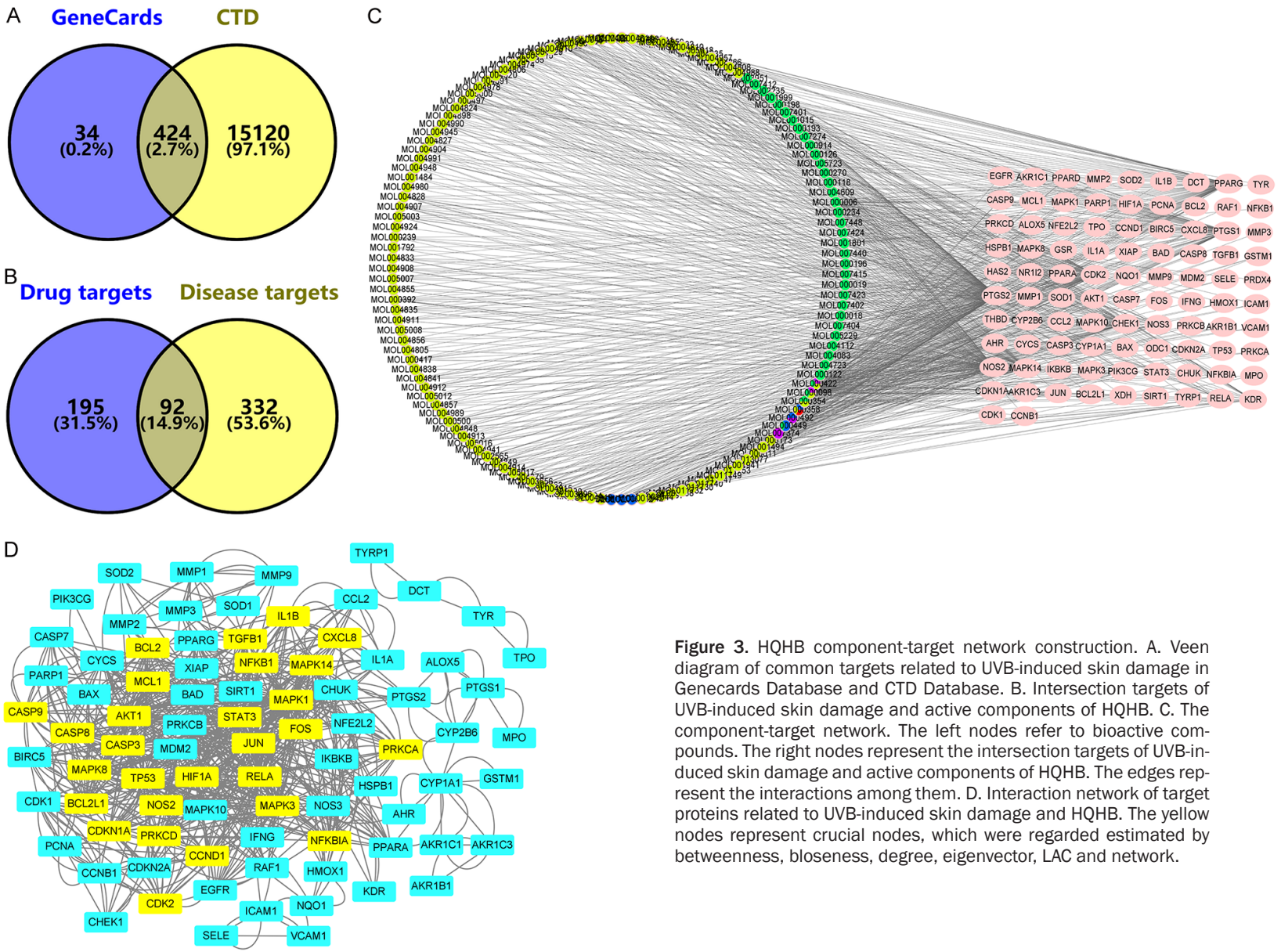

Figure 3. HQHB component-target network construction. A. Veen diagram of common targets related to UVB-induced skin damage in Genecards Database and CTD Database. B. Intersection targets of UVB-induced skin damage and active components of HQHB. C. The component-target network. The left nodes refer to bioactive compounds. The right nodes represent the intersection targets of UVB-induced skin damage and active components of HQHB. The edges represent the interactions among them. D. Interaction network of target proteins related to UVB-induced skin damage and HQHB. The yellow nodes represent crucial nodes, which were regarded estimated by betweenness, bloseness, degree, eigenvector, LAC and network.

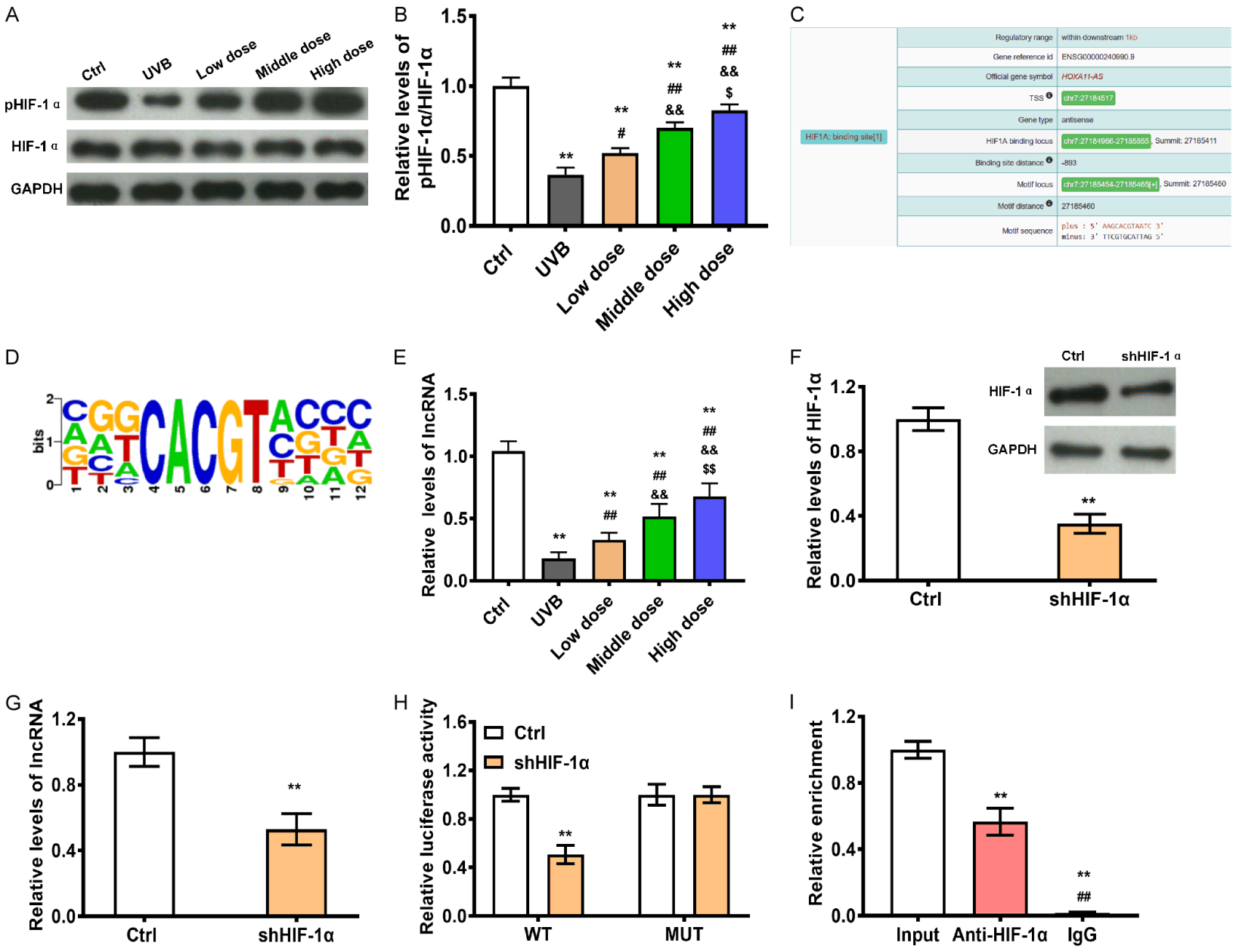
A
Ctrl
UVB
Low dose
Middle dose
High dose
pHIF-1 α
HIF-1 α
GAPDH
B
Relative levels of pHIF-1α/HIF-1α
Ctrl
UVB
Low dose
Middle dose
High dose
C
HIF1A: binding site[1]
Regulatory range
within downstream 1kb
Gene reference id
ENSG00000240990.9
Official gene symbol
HOXA11-AS
TSS
chr7:27184517
Gene type
antisense
HIF1A binding locus
chr7:27184966-27185855 Summit: 27185411
Binding site distance
-893
Motif locus
chr7:27185454-27185465[+] Summit: 27185460
Motif distance
27185460
Motif sequence
plus : 5' AAGCACGTAATC 3'
minus: 3' TTCGTGCATTAG 5'
D
bits
E
Relative levels of lncRNA
Ctrl
UVB
Low dose
Middle dose
High dose
F
Ctrl
shHIF-1 α
HIF-1 α
GAPDH
Relative levels of HIF-1α
Ctrl
shHIF-1α
G
Relative levels of lncRNA
Ctrl
shHIF-1α
H
Ctrl
shHIF-1α
Relative luciferase activity
WT
MUT
I
Relative enrichment
Input
Anti-HIF-1α
IgG

Figure 4. HQHB upregulates HOXA11-AS expression via HIF-1α. A and B. HIF-1α expression in UVB-irradiated skin tissues was measured by western blotting. *P<0.05, **P<0.01 vs Ctrl; #P<0.05, ##P<0.01 vs UVB; &P<0.05, &&P<0.01 vs Low dose; $P<0.05, $$P<0.01 vs Middle dose. C and D. The downstream targets of HIF-1α were predicted by ChIPBase v2.0. E. HOXA11-AS levels in UVB-irradiated skin tissues were measured by qRT-PCR. *P<0.05, **P<0.01 vs Ctrl; #P<0.05, ##P<0.01 vs UVB; &P<0.05, &&P<0.01 vs Low dose; $P<0.05, $$P<0.01 vs Middle dose. F. HIF-1α expression in HaCaT cells with shRNA was determined by western blotting. *P<0.05, **P<0.01 vs Ctrl. G. HOXA11-AS levels in HaCaT cells with shRNA infection of HIF-1α were measured by qRT-PCR. *P<0.05, **P<0.01 vs Ctrl. H. Luciferase activities of chr7:27185454-27185465-wt/mut were quantified in HEK-293T cells transfection with shHIF-1α. *P<0.05, **P<0.01 vs Ctrl. I. ChIP assay in HaCaT cells, followed by qRT-PCR amplification of binding sites within the HOXA11-AS promoter region. *P<0.05, **P<0.01 vs Input; #P<0.05, ##P<0.01 vs Anti-HID-1α.

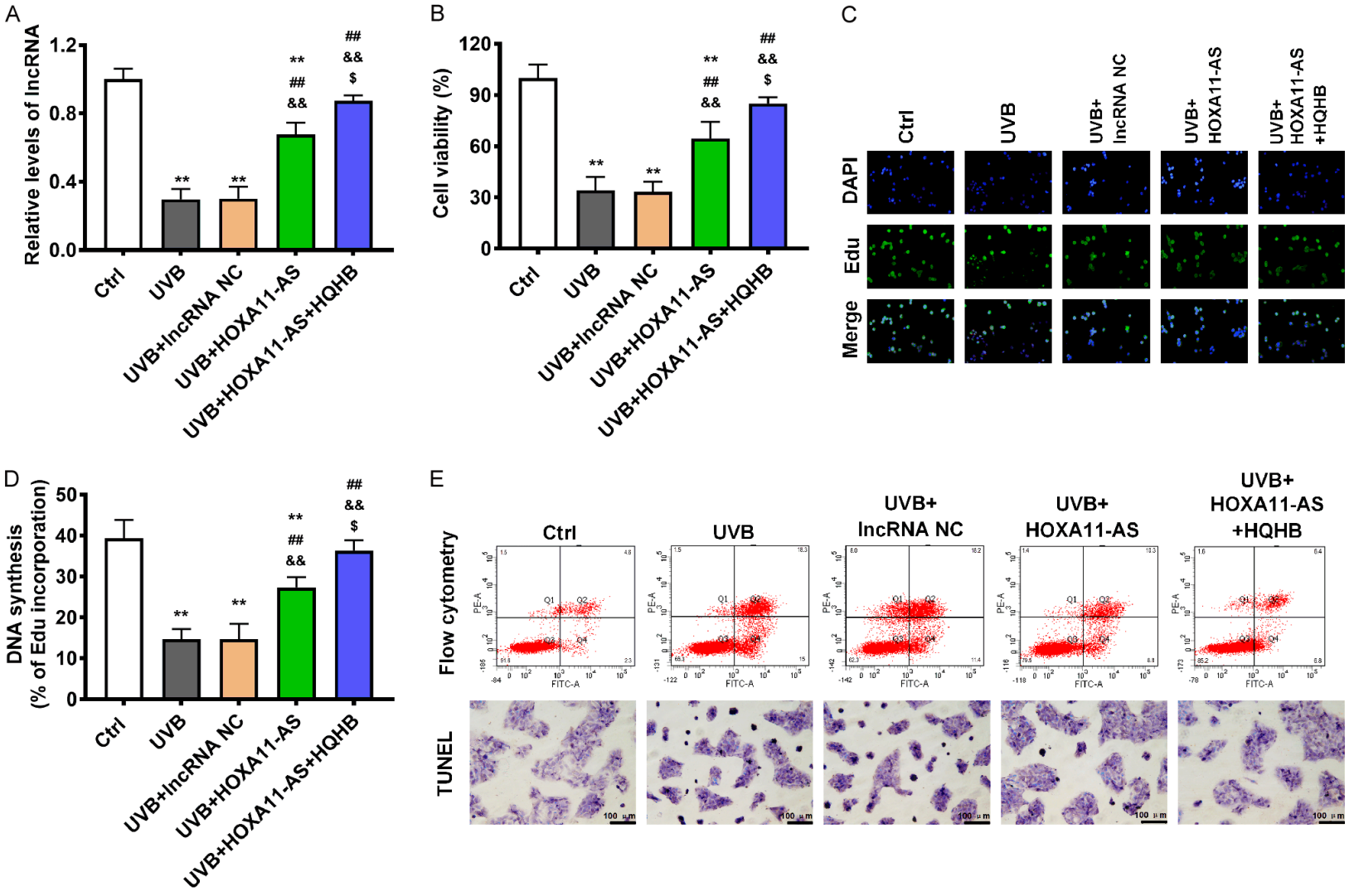

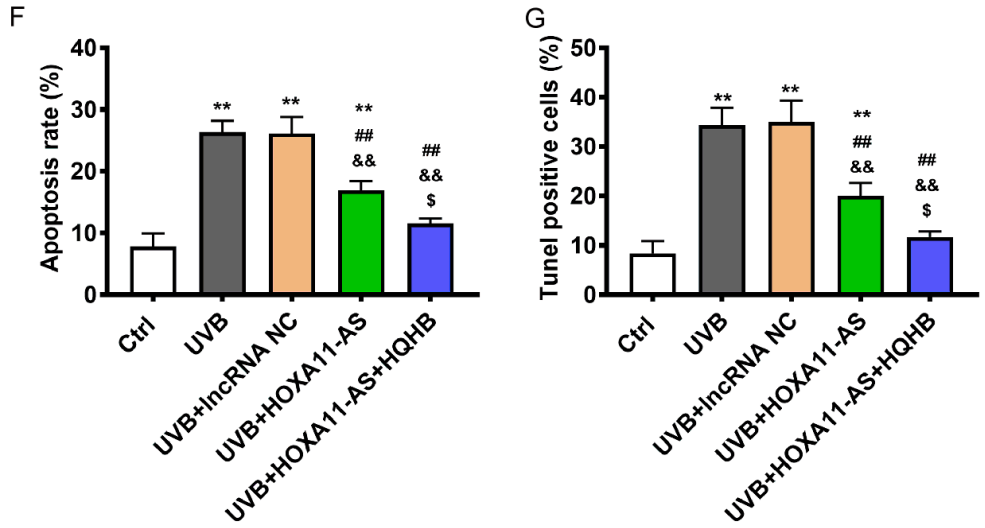

Figure 5. HOXA11-AS reduces UVB-induced cell damage. A. HOXA11-AS expression was examined by qRT-PCR in HaCaT cells overexpressing HOXA11-AS and/or irradiated by UVB. *P<0.05, **P<0.01 vs Ctrl; $^{\#}$P<0.05, $^{\#\#}$P<0.01 vs UVB; $^{\&}$P<0.05, $^{\&\&}$P<0.01 vs UVB+lncRNA NC; $^{\$}$P<0.05, $^{\$\$}$P<0.01 vs UVB+HOXA11-AS. B. Cell proliferation was measured by the CCK8 assay in HaCaT cells overexpressing HOXA11-AS and/or irradiated by UVB. *P<0.05, **P<0.01 vs Ctrl; $^{\#}$P<0.05, $^{\#\#}$P<0.01 vs UVB; $^{\&}$P<0.05, $^{\&\&}$P<0.01 vs UVB+lncRNA NC; $^{\$}$P<0.05, $^{\$\$}$P<0.01 vs UVB+HOXA11-AS. C and D. Cell proliferation was investigated by the EdU incorporation assays in HaCaT cells overexpressing HOXA11-AS and/or irradiated by UVB (×100). *P<0.05, **P<0.01 vs Ctrl; $^{\#}$P<0.05, $^{\#\#}$P<0.01 vs UVB; $^{\&}$P<0.05, $^{\&\&}$P<0.01 vs UVB+lncRNA NC; $^{\$}$P<0.05, $^{\$\$}$P<0.01 vs UVB+HOXA11-AS. E and F. Cell apoptosis was investigated by flow cytometry of HaCaT cells overexpressing HOXA11-AS and/or irradiated by UVB. Scale bars, 100 μm. *P<0.05, **P<0.01 vs Ctrl; $^{\#}$P<0.05, $^{\#\#}$P<0.01 vs UVB; $^{\&}$P<0.05, $^{\&\&}$P<0.01 vs UVB+lncRNA NC; $^{\$}$P<0.05, $^{\$\$}$P<0.01 vs UVB+HOXA11-AS. E and G. Cell apoptosis was investigated by TUNEL stain analysis in HaCaT cells overexpressing HOXA11-AS and/or irradiated by UVB. *P<0.05, **P<0.01 vs Ctrl; $^{\#}$P<0.05, $^{\#\#}$P<0.01 vs UVB; $^{\&}$P<0.05, $^{\&\&}$P<0.01 vs UVB+lncRNA NC; $^{\$}$P<0.05, $^{\$\$}$P<0.01 vs UVB+HOXA11-AS.

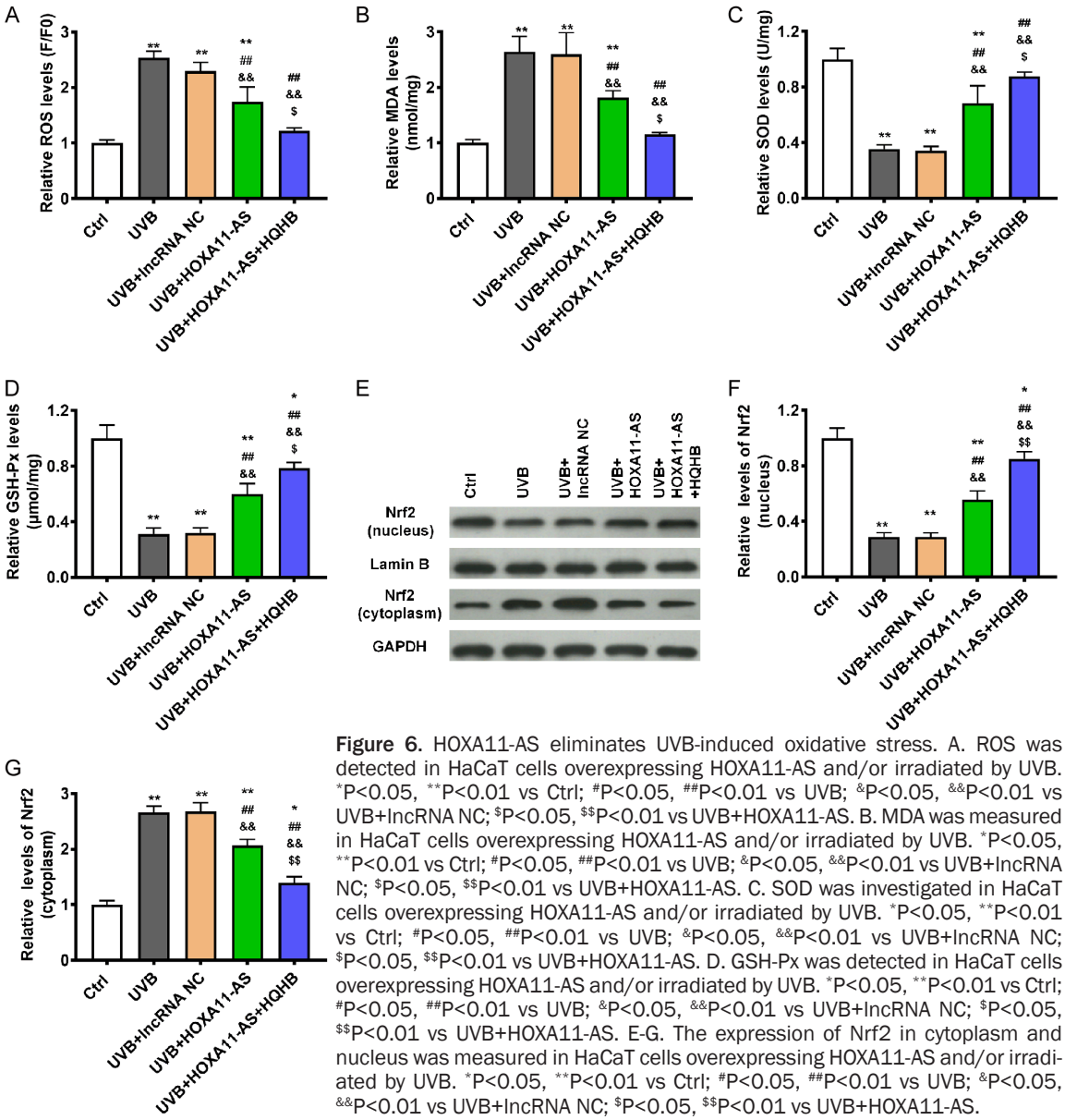

Figure 6. HOXA11-AS eliminates UVB-induced oxidative stress. A. ROS was detected in HaCaT cells overexpressing HOXA11-AS and/or irradiated by UVB. *P<0.05, **P<0.01 vs Ctrl; $^{\#}$P<0.05, $^{\#\#}$P<0.01 vs UVB; $^{\&}$P<0.05, $^{\&\&}$P<0.01 vs UVB+lncRNA NC; $^{\$}$P<0.05, $^{\$\$}$P<0.01 vs UVB+HOXA11-AS. B. MDA was measured in HaCaT cells overexpressing HOXA11-AS and/or irradiated by UVB. *P<0.05, **P<0.01 vs Ctrl; $^{\#}$P<0.05, $^{\#\#}$P<0.01 vs UVB; $^{\&}$P<0.05, $^{\&\&}$P<0.01 vs UVB+lncRNA NC; $^{\$}$P<0.05, $^{\$\$}$P<0.01 vs UVB+HOXA11-AS. C. SOD was investigated in HaCaT cells overexpressing HOXA11-AS and/or irradiated by UVB. *P<0.05, **P<0.01 vs Ctrl; $^{\#}$P<0.05, $^{\#\#}$P<0.01 vs UVB; $^{\&}$P<0.05, $^{\&\&}$P<0.01 vs UVB+lncRNA NC; $^{\$}$P<0.05, $^{\$\$}$P<0.01 vs UVB+HOXA11-AS. D. GSH-Px was detected in HaCaT cells overexpressing HOXA11-AS and/or irradiated by UVB. *P<0.05, **P<0.01 vs Ctrl; $^{\#}$P<0.05, $^{\#\#}$P<0.01 vs UVB; $^{\&}$P<0.05, $^{\&\&}$P<0.01 vs UVB+lncRNA NC; $^{\$}$P<0.05, $^{\$\$}$P<0.01 vs UVB+HOXA11-AS. E-G. The expression of Nrf2 in cytoplasm and nucleus was measured in HaCaT cells overexpressing HOXA11-AS and/or irradiated by UVB. *P<0.05, **P<0.01 vs Ctrl; $^{\#}$P<0.05, $^{\#\#}$P<0.01 vs UVB; $^{\&}$P<0.05, $^{\&\&}$P<0.01 vs UVB+lncRNA NC; $^{\$}$P<0.05, $^{\$\$}$P<0.01 vs UVB+HOXA11-AS.

We also examined the effect of HOXA11-AS on the expression of Nrf2. Nrf2 expression was significantly reduced in the cytoplasm and elevated in the nuclei of HaCaT cells that overexpressed HOXA11-AS as compared with those irradiated by UVB (P<0.01, **Figure 6E-G**). When compared with HOXA11-AS overexpression, Nrf2 expression was further significantly reduced in the cytoplasm and elevated in the nuclei of HaCaT cells treated with HOXA11-AS overexpression and HQHB administration (P<0.01, **Figure 6E-G**). Therefore, we confirmed that HOXA11-AS was responsible for the beneficial effect of HQHB on skin damage induced by UVB.

HOXA11-AS inhibited ubiquitin-proteasome degradation of EZH2

To explore the molecular mechanisms of HOXA11-AS in HaCaT cells, we first investigated its distribution in cells by nucleocytoplasmic separation. The results of **Figure 7A** demonstrated that HOXA11-AS was localized mostly in the cytoplasm, but there were also a few cells that exhibited HOXA11-AS expression in the nucleus. Using the RNAInter database (http://www.rna-society.org/rnainter/home.html), 181 targets binding HOXA11-AS were found (**Figure 7B**). Given that EZH2 was associated with oxidative stress [17], we further evaluated the

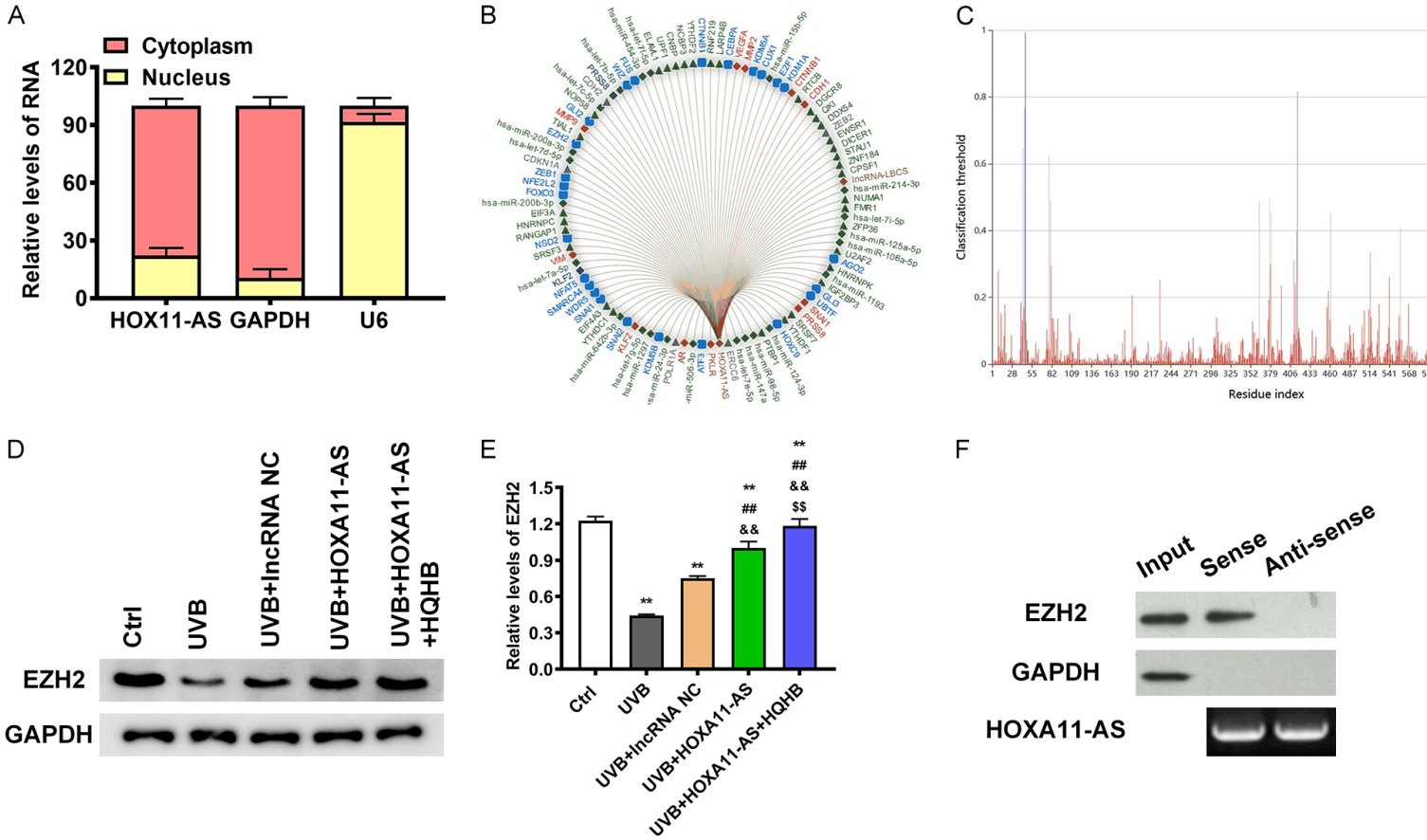
A
Cytoplasm
Nucleus
Relative levels of RNA
120
90
60
30
0
HOX11-AS
GAPDH
U6
B
C
Classification threshold
Residue index
D
Ctrl
UVB
UVB+lncRNA NC
UVB+HOXA11-AS
UVB+HOXA11-AS +HQHB
EZH2
GAPDH
E
Relative levels of EZH2
Ctrl
UVB
UVB+lncRNA NC
UVB+HOXA11-AS
UVB+HOXA11-AS+HQHB
F
Input
Sense
Anti-sense
EZH2
GAPDH
HOXA11-AS
G
EZH2
IgG
RIP (% of input)
GAPDH
HOXA11-AS
H
MG132
0 h
4 h
6 h
Ctrl
EZH2
GAPDH
HOXA11-AS
EZH2
GAPDH
I
HOXA11-AS
Ctrl
Relative levels of EZH2
0 h
3 h
6 h

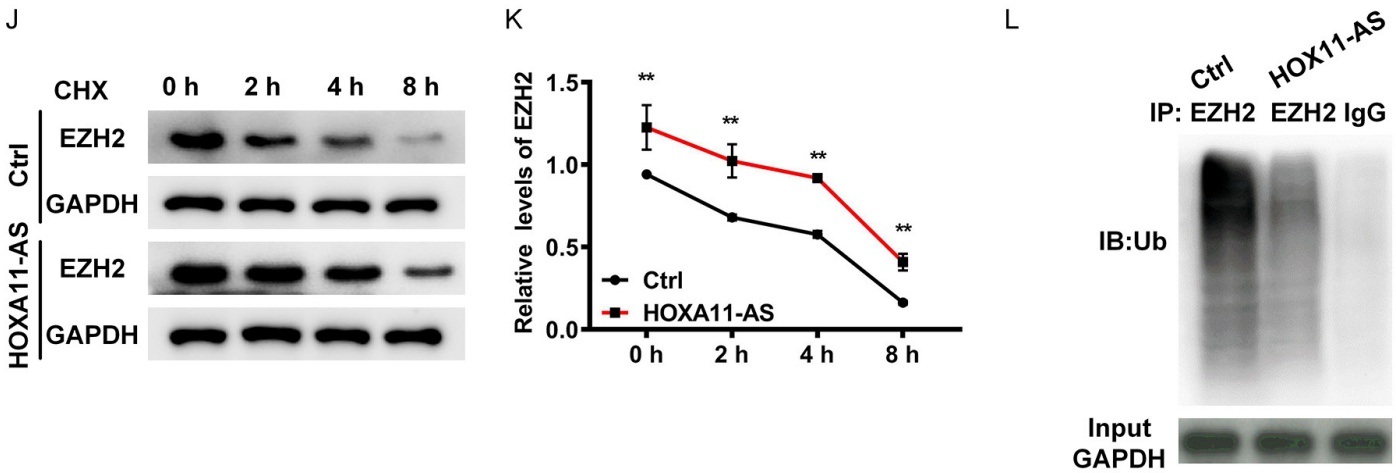

Figure 7. HOXA11-AS interacts with and stabilizes EZH2 protein by inhibiting its ubiquitination. A. HOXA11-AS levels in nuclear and cytoplasm of HaCaT cells were detected by qRT-PCR. B and C. The downstream targets of HOXA11-AS were predicted by RNAInter. D and E. EZH2 expression was detected by western blotting in HaCaT cells after HOXA11-AS overexpression in cells damaged by UVB. *P<0.05, **P<0.01 vs Ctrl; $^{\#}$P<0.05, $^{\#\#}$P<0.01 vs UVB; $^{\&}$P<0.05, $^{\&\&}$P<0.01 vs UVB+lncRNA NC; $^{\$}$P<0.05, $^{\$\$}$P<0.01 vs UVB+HOXA11-AS. F. HaCaT cell lysates were mixed with biotinylated HOXA11-AS or antisense, and bound proteins were assessed by western blotting to measure EZH2. G. Lysates of HaCaT cells were used for ChIP with anti-EZH2, with the resultant products being amplified via qRT-PCR. *P<0.05, **P<0.01 vs IgG. H and I. EZH2 was determined by western blotting in HaCaT cells followed by MG132 treatment. *P<0.05, **P<0.01 vs Ctrl; $^{\#}$P<0.05, $^{\#\#}$P<0.01 vs 3 h of Ctrl; $^{\&}$P<0.05, $^{\&\&}$P<0.01 vs 6 h of Ctrl. J and K. EZH2 was determined by western blotting in HaCaT cells followed by CHX treatment at different times. L. EZH2-associated ubiquitination was measured in HaCaT cells followed by HOXA11-AS overexpression. *P<0.05, **P<0.01 vs Ctrl.

effect of HOXA11-AS on EZH2 expression (**Figure 7C**). Western blotting showed that HOXA11-AS overexpression eliminated UVB-induced EZH2 inhibition in HaCaT cells (**Figure 7D**, **7E**). Subsequently, we interrogated the mechanism behind HOXA11-AS negative regulation of EZH2 in HaCaT cells. An RNA pulldown assay demonstrated an enrichment of EZH2 protein on a biotin-labeled probe of HOXA11-AS, but not with HOXA11-AS-antisense (**Figure 7F**). The RIP assay showed that HOXA11-AS was highly expressed on the RNA-protein complex immunoprecipitated by anti-EZH2 (**Figure 7G**), confirming an interplay between EZH2 and HOXA11-AS. To determine whether HOXA11-AS affects EZH2 stability associated with proteasome-mediated degradation, we treated HaCaT cells with MG132, a proteasome inhibitor, to prevent EZH2 degradation. In the presence of both HOXA11-AS and MG132, EZH2 protein levels increased significantly (**Figure 7H**, **7I**). Moreover, using the protein synthesis inhibitor cycloheximide (CHX), we found that HOXA11-AS overexpression prolonged the half-life of EZH2 (**Figure 7J**, **7K**). In addition, we immunoprecipitated EZH2 protein from HOXA11-AS overexpressing HaCaT cells and vector cells to investigate ubiquitination of EZH2. The results of **Figure 7L** revealed that EZH2 ubiquitination was significantly inhibited by overexpression of HOXA11-AS. These data indicate that HOXA11-AS stabilizes EZH2 protein by inhibiting its ubiquitination and proteasomal degradation.

Discussion

The effects of various active components of HQHB on the reduction of oxidative stress provide insight into its mechanism of action. Therefore, we investigated the protective effect of HQHB on UVB-induced skin damage, as well as its possible mechanisms. Our findings indicate that HQHB administration inhibits UVB-induced skin damage in mice, including reducing epidermal edema and inhibiting cell apoptosis. Moreover, HQHB administration was capable of restoring the impaired antioxidant defense system. Subsequently, we validated that HQHB upregulated HOXA11-AS expression by activating HIF-1α. HOXA11-AS was found to have an ability to stabilize EZH2 protein by inhibiting its ubiquitination and proteasomal degradation. In addition, HOXA11-AS was involved in a protective effect against skin damage caused by UVB through blocking oxidative stress.

PLE is one of the most common photodermatoses in all types of skin [18]. Ahmed et al. [19] found that UVA-induced differential modulation of antioxidant enzymes and oxidative stress in PLE might play a pathogenic role, which supports the incorporation of antioxidant drugs in the PLE treatment protocol. At present, the induction of immune tolerance by photochemotherapy and phototherapy are useful PLE prophylactic methods in moderate to severe cases [20]. However, some subjects experience disease exacerbation during treatment. Furthermore, the suppression of PLE is also temporary, with clinical efficacy usually lasting approximately 5 weeks [2]. Therefore, it is urgent to find a quick and effective systemic agent for PLE treatment. In the present study we found that HQHB administration inhibits UVB-induced skin damage in mice, including reducing epidermal thickness and inhibiting cell apoptosis. These findings suggest that HQHB may be effective for prevention of UVB-induced skin damage. Evidence shows that the pathogenesis of PLE may be involved in UVA-induced oxidative stress [19, 21]. Since Almudena Pérez-Sánchez et al. [22] reported UVB-induced DNA damage and oxidative stress in a skin cell model, we explored the ability of HQHB to alleviate oxidative stress. We found that UVB irradiation impaired antioxidant defenses, which could be restored by HQHB treatment in a dose-dependent manner. These results indicated that HQHB attenuation of UVB-induced skin damage is achieved by inhibition of oxidative stress, which expands the application of HQHB in novel sun protection strategies. Given the significance of immune responses in PLE, we still need to explore the regulation of HQHB on immune responses in PLE in the future.

At present, the mechanism of HQHB inhibition of UVB-induced oxidative stress remains unclear. To further broaden our investigation into the mechanism of HQHB functioning in oxidative stress, we investigated the downstream targets of HQHB through network pharmacology. Interestingly, 173 components of HQHB were identified, while 92 genes, that were both related to the components of HQHB and UVB-induced skin damage, were identified. Through the potential inter-protein interactions,

the most important targets in the network contain 28 genes. HIF-1α aroused our interest as it was previously shown that HIF-1α protects against oxidative stress by directly targeting mitochondria [23]. Our research confirmed that HQHB activates HIF-1α in a dose-dependent manner, consistent with a recent report in which Herba Artemisiae Annuae induced the phosphorylation of HIF-1α in a calcium-dependent manner [24]. LncRNAs serve as important regulators of various biologic processes in the pathogenesis and progression of a variety of medical conditions, including skin damage [25-27]. For example, data from Zhang's study [28] showed that the lncRNA Meg3 activates inflammatory damage by the sponging miR-93-5p/epiregulin axis in UVB-induced murine skin lesions. Zhao et al. [29] found that lncRNA HULC up-regulated BNIP3 and activated the JAK/STAT (1/3) pathway to increase UVB-induced cell damage. Therefore, we predicted the transcriptional regulation of lncRNA by HIF-1α. In our current study, we confirmed that HIF-1α induces the up-regulation of HOXA11-AS through binding the HOXA11-AS promoter. HOXA11-AS, the antisense strand of the HOXA11 gene, was initially found in a mouse embryonic cDNA library [30]. A growing body of research has shown that aberrant HOXA11-AS expression can play a key role in regulating cell proliferation and apoptosis [31-33]. Using rescue assays we found that HOXA11-AS boosted proliferation and inhibited apoptosis in HaCaT cells, consistent with findings in LUAD cells [34]. Interestingly, compared to HOXA11-AS overexpression, we found that HOXA11-AS overexpression combined with HQHB further increased cell proliferation and inhibited cell apoptosis in HaCaT cells. Subsequently, we confirmed, for the first time, a role for HOXA11-AS in alleviating oxidative stress. While HOXA11-AS overexpression combined with HQHB further alleviated oxidative stress. Our results reveal a new mechanism underlying HQHB alleviation of UVB-induced skin damage.

Little is known about how HOXA11-AS regulates oxidative stress. It has been reported that USF1-induced LINC01048 upregulation promotes cell proliferation and inhibits apoptosis by binding to TAF15 to transcriptionally activate YAP1 in cutaneous squamous cell carcinoma [35]. Furthermore, lncRNA GAS5 was found to accelerate oxidative stress in melanoma cells by rescuing EZH2-mediated CDKN1C downregulation [17]. In line with this, we predicted and confirmed that HOXA11-AS interacts with EZH2 in HaCaT cells, consistent with Liu's report [36]. More recently, a set of studies have demonstrated the critical role of EZH2 in oxidative stress [17, 37]. For example, Liu et al. [38] found that inhibition of EZH2 alleviated renal pyroptosis by impeding Nox4-mediated ROS generation through the ALK5/Smad2/3 pathway. Wan et al. [39] reported that inhibition of EZH2 alleviates angiogenesis by blocking FoxO3a-mediated oxidative stress in a model of corneal neovascularization. However, how the interaction between HOXA11-AS and EZH2 might influence EZH2 levels remains unclear. We also found that HOXA11-AS stabilized the EZH2 protein by inhibiting its ubiquitination and subsequent proteasomal degradation, consistent with previous studies in which knockdown of EZH2 expression could reverse HOXA11-AS-induced biologic behavior in hepatocellular carcinoma cells [40]. These findings identify HQHB/HIF-1/HOXA11-AS/EZH2 regulatory networks, highlighting the importance of HQHB in the prevention and treatment of PLE.

Overall, this study can be summarized by the following major findings: (a) We confirmed that HQHB successfully alleviates UVB-induced skin damage by eliminating oxidative stress in a dose-dependent manner. (b) We verified that HQHB-activated HIF-1α induces the up-regulation of HOXA11-AS. (c) We demonstrated that HOXA11-AS interacts with and stabilizes EZH2 protein by inhibiting its ubiquitination. (d) We confirmed that HOXA11-AS acts against UVB-induced skin damage by blocking oxidative stress. These findings indicate that HQHB may be effective in the prevention and treatment of PLE.

Acknowledgements

This study was supported by the Natural Science Foundation of China (81774309).

Disclosure of conflict of interest

None.

Address correspondence to: Liyun Sun, Department of Dermatology, Beijing Hospital of Traditional Chinese Medicine, Capital Medical University, No. 23 Museum Back Street, Dongcheng District, Beijing 100010, China. E-mail: liyunsuncmu@163.com

References

[1] Hönigsmann H. Polymorphous light eruption. Photodermatol Photoimmunol Photomed 2008; 24: 155-161.

[2] Stratigos A, Antoniou C and Katsambas A. Polymorphous light eruption. J Eur Acad Dermatol Venereol 2002; 16: 193-206.

[3] Guarrera M. Polymorphous light eruption, in ultraviolet light in human health, diseases and environment. In: Ahmad SI, editor. Cham: Springer International Publishing; 2017. pp. 61-70.

[4] Miguel D and Lindhaus C. Polymorphous light eruption mimicking erythema multiforme. Dtsch Arztebl Int 2018; 115: 627.

[5] Oliveira MM, Ratti BA, Daré RG, Silva SO, Truiti M, Ueda-Nakamura T, Auzély-Velty R and Nakamura CV. Dihydrocaffeic acid prevents UVB-induced oxidative stress leading to the inhibition of apoptosis and MMP-1 expression via p38 signaling pathway. Oxid Med Cell Longev 2019; 2019: 2419096.

[6] Aristatile B, Al-Numair KS, Al-Assaf AH, Veeramani C and Pugalendi KV. Protective effect of carvacrol on oxidative stress and cellular DNA damage induced by UVB irradiation in human peripheral lymphocytes. J Biochem Mol Toxicol 2015; 29: 497-507.

[7] Shi S, Zheng G, Yang C, Chen X, Yan Q, Jiang F, Jiang X, Xin Y and Jiang G. Effects of vitamin K3 combined with UVB on the proliferation and apoptosis of cutaneous squamous cell carcinoma A431 cells. Onco Targets Ther 2019; 12: 11715-11727.

[8] Hong Y, Sun Y, Rong X, Li D, Lu Y and Ji Y. Exosomes from adipose-derived stem cells attenuate UVB-induced apoptosis, ROS, and the Ca(2+) level in HLEC cells. Exp Cell Res 2020; 396: 112321.

[9] Wang J, Wong YK and Liao F. What has traditional Chinese medicine delivered for modern medicine? Expert Rev Mol Med 2018; 20: e4.

[10] Liu SH, Chuang WC, Lam W, Jiang Z and Cheng YC. Safety surveillance of traditional Chinese medicine: current and future. Drug Saf 2015; 38: 117-28.

[11] Wu Y, Wang D, Yang X, Fu C, Zou L and Zhang J. Traditional Chinese medicine Gegen Qinlian decoction ameliorates irinotecan chemotherapy-induced gut toxicity in mice. Biomed Pharmacother 2019; 109: 2252-2261.

[12] Dan F, Ting L, Guanru L and Liyun S. Effects of Haoqin Huaban formula on photic injury of HaCaT cells induced by ultraviolet-B. Global Traditional Chinese Medicine 2020; 13: 778-783.

[13] Tanaka M, Kishimoto Y, Sasaki M, Sato A, Kamiya T, Kondo K and Iida K. Terminalia bellirica (gaertn.) roxb. extract and gallic acid attenuate LPS-induced inflammation and oxidative stress via MAPK/NF-κB and Akt/AMPK/Nrf2 pathways. Oxid Med Cell Longev 2018; 2018: 9364364.

[14] Gou SH, He M, Li BB, Zhu NY and Ni JM. Hepatoprotective effect of total flavonoids from Glycyrrhiza uralensis Fisch in liver injury mice. Nat Prod Res 2020; 35: 6083-6087.

[15] Zhang Y, Wang C, Lu J, Jin Y, Xu C, Meng Q, Liu Q, Dong D, Ma X, Liu K and Sun H. Targeting of miR-96-5p by catalpol ameliorates oxidative stress and hepatic steatosis in LDLr-/- mice via p66shc/cytochrome C cascade. Aging (Albany NY) 2020; 12: 2049-2069.

[16] Feng D, Liu T, Li G and Sun L. Effects of Haoqin Huaban formula on photic injury of HaCaT cells induced by ultraviolet-B. Global Traditional Chinese Medicine 2020; 13: 27-32.

[17] Xu W, Yan Z, Hu F, Wei W, Yang C and Sun Z. Long non-coding RNA GAS5 accelerates oxidative stress in melanoma cells by rescuing EZH2-mediated CDKN1C downregulation. Cancer Cell Int 2020; 20: 116.

[18] Libon F and Nikkels AF. Polymorphous light eruption: phototherapy-based desensitization versus intramuscular steroids - who is right, who is wrong? Dermatology 2018; 234: 192-193.

[19] Ahmed RS, Suke SG, Seth V, Jain A, Bhattacharya SN and Banerjee BD. Impact of oral vitamin E supplementation on oxidative stress & lipid peroxidation in patients with polymorphous light eruption. Indian J Med Res 2006; 123: 781-7.

[20] Naleway AL. Polymorphous light eruption. Int J Dermatol 2002; 41: 377-383.

[21] Hadshiew IM, Treder-Conrad C, v Bülow R, Klette E, Mann T, Stäb F, Moll I and Rippke F. Polymorphous light eruption (PLE) and a new potent antioxidant and UVA-protective formulation as prophylaxis. Photodermatol Photoimmunol Photomed 2004; 20: 200-4.

[22] Pérez-Sánchez A, Barrajón-Catalán E, Herranz-López M, Castillo J and Micol V. Lemon balm extract (Melissa officinalis, L.) promotes melanogenesis and prevents UVB-induced oxidative stress and DNA damage in a skin cell model. J Dermatol Sci 2016; 84: 169-177.

[23] Li HS, Zhou YN, Li L, Li SF, Long D, Chen XL, Zhang JB, Feng L and Li YP. HIF-1α protects against oxidative stress by directly targeting mitochondria. Redox Biol 2019; 25: 101109.

[24] Riganti C, Doublier S, Viarisio D, Miraglia E, Pescarmona G, Ghigo D and Bosia A. Artemisinin induces doxorubicin resistance in human colon cancer cells via calcium-dependent activation of HIF-1alpha and P-glycoprotein overexpression. Br J Pharmacol 2009; 156: 1054-66.

[25] Szcześniak MW, Wanowska E, Mukherjee N, Ohler U and Makałowska I. Towards a deeper annotation of human lncRNAs. Biochim Biophys Acta Gene Regul Mech 2020; 1863: 194385.
[26] Brahmbhatt HD, Gupta R, Gupta A, Rastogi S, Misri R, Mobeen A, Ghosh A, Kothari P, Sitaniya S, Scaria V and Singh A. Long non-coding RNA MALAT1 suppresses miR-211 to confer protection from UV-mediated DNA damage in vitiligo epidermis by upregulating SIRT1. Br J Dermatol 2020; 184: 1132-1142.
[27] Nakayama Y, Fujiu K, Yuki R, Oishi Y, Morioka MS, Isagawa T, Matsuda J, Oshima T, Matsubara T, Sugita J, Kudo F, Kaneda A, Endo Y, Nakayama T, Nagai R, Komuro I and Manabe I. A long noncoding RNA regulates inflammation resolution by mouse macrophages through fatty acid oxidation activation. Proc Natl Acad Sci U S A 2020; 117: 14365-14375.
[28] Zhang N, Zhong Z, Wang Y, Yang L, Wu F, Peng C, Huang W and He G. Competing endogenous network analysis identifies lncRNA Meg3 activates inflammatory damage in UVB induced murine skin lesion by sponging miR-93-5p/epiregulin axis. Aging (Albany NY) 2019; 11: 10664-10683.
[29] Zhao L, Man Y and Liu S. Long non-coding RNA HULC promotes UVB-induced injury by up-regulation of BNIP3 in keratinocytes. Biomed Pharmacother 2018; 104: 672-678.
[30] Chau YM, Pando S and Taylor HS. HOXA11 silencing and endogenous HOXA11 antisense ribonucleic acid in the uterine endometrium. J Clin Endocrinol Metab 2002; 87: 2674-80.
[31] Sun M, Nie F, Wang Y, Zhang Z, Hou J, He D, Xie M, Xu L, De W, Wang Z and Wang J. LncRNA HOXA11-AS promotes proliferation and invasion of gastric cancer by scaffolding the chromatin modification factors PRC2, LSD1, and DNMT1. Cancer Res 2016; 76: 6299-6310.
[32] Niu X, Yang B, Liu F and Fang Q. LncRNA HOXA11-AS promotes OSCC progression by sponging miR-98-5p to upregulate YBX2 expression. Biomed Pharmacother 2020; 121: 109623.
[33] Li Y, Yan G, Zhang J, Chen W, Ding T, Yin Y, Li M, Zhu Y, Sun S, Yuan JH and Guo Z. LncRNA HOXA11-AS regulates calcium oxalate crystal-induced renal inflammation via miR-124-3p/MCP-1. J Cell Mol Med 2020; 24: 238-249.
[34] Zhao X, Li X, Zhou L, Ni J, Yan W, Ma R, Wu J, Feng J and Chen P. LncRNA HOXA11-AS drives cisplatin resistance of human LUAD cells via modulating miR-454-3p/Stat3. Cancer Sci 2018; 109: 3068-3079.
[35] Chen L, Chen Q, Kuang S, Zhao C, Yang L, Zhang Y, Zhu H and Yang R. USF1-induced upregulation of LINC01048 promotes cell proliferation and apoptosis in cutaneous squamous cell carcinoma by binding to TAF15 to transcriptionally activate YAP1. Cell Death Dis 2019; 10: 296.
[36] Liu Z, Chen Z, Fan R, Jiang B, Chen X, Chen Q, Nie F, Lu K and Sun M. Over-expressed long noncoding RNA HOXA11-AS promotes cell cycle progression and metastasis in gastric cancer. Mol Cancer 2017; 16: 82.
[37] Gao M, Liu Y, Chen Y, Yin C, Chen JJ and Liu S. miR-214 protects erythroid cells against oxidative stress by targeting ATF4 and EZH2. Free Radic Biol Med 2016; 92: 39-49.
[38] Liu H, Chen Z, Weng X, Chen H, Du Y, Diao C, Liu X and Wang L. Enhancer of zeste homolog 2 modulates oxidative stress-mediated pyroptosis in vitro and in a mouse kidney ischemia-reperfusion injury model. FASEB J 2020; 34:835-852.
[39] Wan SS, Pan YM, Yang WJ, Rao ZQ and Yang YN. Inhibition of EZH2 alleviates angiogenesis in a model of corneal neovascularization by blocking FoxO3a-mediated oxidative stress. FASEB J 2020; 34: 10168-10181.
[40] Zhang WL, Zhao YN, Shi ZZ, Gu GY, Cong D, Wei C and Bai YS. HOXA11-AS promotes the migration and invasion of hepatocellular carcinoma cells by inhibiting miR-124 expression by binding to EZH2. Hum Cell 2019; 32: 504-514.